Abyssal hill characterization at the ultraslow spreading Southwest Indian Ridge

Heather Sloan, Daniel Sauter, John A. Goff, Mathilde Cannat

Abyssal hill characterization at the ultraslow spreading Southwest Indian Ridge

Heather Sloan

Environmental, Geographic and Geological Sciences, Lehman College, City University of New York, 250 Bedford Park Boulevard West, Bronx, New York 10468, USA (heather.sloan@lehman.cuny.edu)

Daniel Sauter

Institut de Physique du Globe de Strasbourg, IPGS–UMR 7516, CNRS, Université de Strasbourg/ EOST, 1 rue Blessig, F-67084 Strasbourg CEDEX, France (daniel.sauter@unistra.fr)

John A. Goff

Institute for Geophysics, Jackson School of Geosciences, University of Texas at Austin, 10100 Burnet Road, Austin, Texas 78758, USA (goff@utig.ig.utexas.edu)

Mathilde Cannat

Equipe de Géosciences Marines, CNRS–UMR 7154, Institut de Physique du Globe de Paris, 4 place Jussieu, F-75252 Paris CEDEX 05, France (cannat@ipgp.jussieu.fr)

[1] The morphology of the flanks of the Southwest Indian Ridge holds a record of seafloor formation and abyssal hill generation at an ultraslow spreading rate. Statistical analysis of compiled bathymetry and gravity data from the flanks of the Southwest Indian Ridge from 54°E to 67°E provides estimates of abyssal hill morphologic character and inferred crustal thickness. The extent of the compiled data encompasses a spreading rate change from slow to ultraslow at ~24 Ma, a significant inferred variation in sub-axis mantle temperature, and a patchwork of volcanic and non-volcanic seafloor, making the Southwest Indian Ridge an ideal and unique location to characterize abyssal hills generated by ultraslow spreading and to examine the effect of dramatic spreading rate change on seafloor morphology. Root mean square abyssal hill height in ultraslow spreading seafloor ranges from ~280 m to ~320 m and is on average ~80 m greater than found for slow-spreading seafloor. Ultraslow spreading abyssal hill width ranges from ~4 km to ~12 km, averaging ~8 km. Abyssal hill height and width increases west-to-east in both slow and ultraslow spreading seafloor, corresponding to decreasing inferred mantle temperature. Abyssal hills persist in non-volcanic seafloor and extend continuously from volcanic to non-volcanic terrains. We attribute the increase of abyssal hill height and width to strengthening of the mantle portion of the lithosphere as the result of cooler sub-axial mantle temperature and conclude that abyssal hill height is primarily controlled by the strength of the mantle component of the lithosphere rather than spreading rate.

Theme: From the Mantle to the Ocean: Life, Energy, and Material Cycles at Slow
Spreading Ridges

1. Introduction

[2]   The characteristics of abyssal hills at ultraslow spreading ridges and how they compare to seafloor generated at faster rates have not been extensively explored. Abyssal hills are the most pervasive geologic feature on the planet, covering 85% or more of the seafloor [*Menard*, 1960, 1967; *Goff*, 1992]. However, only a small fraction of the seafloor has been mapped with the resolution necessary to characterize abyssal hill fabric reliably. The majority of high-resolution bathymetric surveys at intermediate and slower spreading ridges are sited on or near the ridge axis rather than the ridge flanks where the formation of abyssal hill fabric can be assumed to be complete [e.g., *Sauter et al.*, 1996; *Shaw and Lin*, 1993; *Sloan and Patriat*, 2004]. Although limited, these data have been enough to drive the development of multiple models of abyssal hill formation. Conceptual models based on interpretation of observations and more abstract quantitative calculations attribute abyssal hill character primarily to lithosphere strength, spreading rate, and sub-axial magma supply [e.g., *Buck and Poliakov*, 1998; *Buck et al.*, 1997, 2005; *Cannat et al.*, 2003; *Goff*, 1991, 1992; *Goff and Jordan*, 1988; *Goff et al.*, 1993, 1995, 1997; *Malinverno*, 1991; *Malinverno and Pockalny*, 1990; *Neumann and Forsyth*, 1995; *Poliakov and Buck*, 1998; *Sloan and Patriat*, 2004; *Tucholke et al.*, 1997].

[3]   The dependence of lithosphere character on spreading rate is widely accepted: slower spreading rates tend to produce thicker, stronger lithosphere [e.g., *Lin and Parmentier*, 1989; *Lin and Phipps Morgan*, 1992]. Several models for abyssal hill generation link lithosphere thickness and strength with normal fault throw, fault spacing or frequency, and elastic flexure [e.g., *Buck et al.*, 2005; *Buck and Poliakov*, 1998; *Shaw and Lin*, 1993]. Thicker, stronger lithosphere is thought to sustain greater fault spacing, throw, and elastic flexure to produce larger abyssal hills. Thus, slower spreading rates should produce larger abyssal hills than are typically generated at intermediate and fast spreading

rates [e.g., *Buck and Poliakov*, 1998; *Chen and Morgan*, 1990; *Goff*, 1991; *Goff et al.*, 1995; *MacDonald et al.*, 1996] with the largest abyssal hills being generated at ultraslow spreading ridges. Comparative observations from the near-axis region and occasionally the flanks of a variety of ridges, in addition to being consistent with the proposed models mentioned above, have generated quantitative predictive models relating abyssal hill morphology to spreading rate [e.g., *Ehlers and Jokat*, 2009; *Malinverno*, 1991]. It must be taken into consideration, however, that these models are based on compilations of widely spaced, isolated data from ridges with a broad range of spreading rates [e.g., *Ehlers and Jokat*, 2009; *Malinverno*, 1991]. To truly test the relationship between spreading rate and abyssal hills size, it is necessary to characterize a full range of abyssal hills generated at distinctly different spreading rates at a single ridge. The Southwest Indian Ridge (SWIR; Figure 1), the focus of this work, underwent a dramatic change from slow (30 mm/yr) to ultraslow (15 mm/yr) spreading ~24 Ma [*Patriat et al.*, 2008]. Compiled bathymetric data from the axis and flanks of the SWIR currently offer the only opportunity to systematically test the effect of slow to ultraslow spreading rate change on abyssal hill morphology.

[4]   The volume of magma supplied to the ridge axis may be another factor contributing to the character of the abyssal hill fabric [e.g., *Behn and Ito*, 2008; *Cannat et al.*, 2008; *Shaw and Lin*, 1996]. Magma supply has been closely linked to sub-axial mantle temperature [e.g., *Cannat et al.*, 2006], making the thermal structure of the ridge system a first-order controlling factor of abyssal hill morphology. Regional (100 s km) variation of sub-axial mantle temperature may affect overall lithosphere thickness as well as the relative thicknesses of its crustal and mantle components [e.g., *Cannat et al.*, 2006]. Geophysical and geochemical data along the SWIR indicate large-scale variation of sub-axial thermal structure (Figure 2) [*Cannat et al.*, 2008; *Sauter and Cannat*, 2010; *Sauter et al.*, 2011a]. Within the study area, mantle temperature is thought to cool
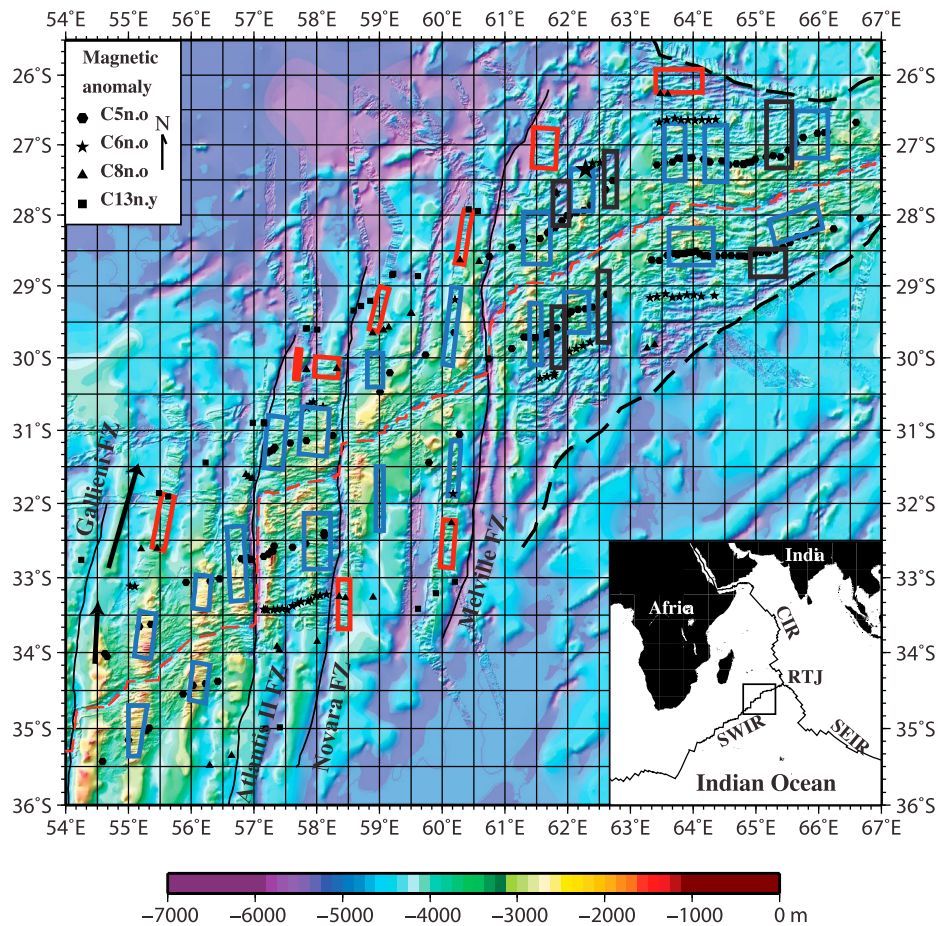
Figure 1. Compiled multibeam bathymetry of the Southwest Indian Ridge between the Gallieni FZ and 67°E with location map inset. Magnetic anomaly identifications A6 (stars), A8 (triangles) and A13 (squares) are from *Patriat et al.* [2008] and *Sauter et al.* [2008], A5 (hexagons) are from *Lemaux et al.* [2002]. Boxes indicate the areas of seafloor selected for morphologic analysis: slow segment center (red), ultraslow volcanic segment center (blue), and non-volcanic seafloor (black). A dashed red line marks the SWIR axis; thin black lines represent transform fault and fracture zones; thick dashed lines represent the triple junction trace; and black arrows indicate plate motion vectors. SWIR: Southwest Indian Ridge; SEIR: Southeast Indian Ridge; CIR: Central Indian Ridge; RTJ: Rodrigues Triple Junction.

progressively west-to-east [*Cannat et al.*, 2008; *Sauter and Cannat*, 2010; *Sauter et al.*, 2011a]. The easternmost part of the SWIR appears to be among the deepest parts of the oceanic ridge system, and it is thus inferred to represent a relatively colder, melt-poor end-member of this system [*Cannat et al.*, 1999]. The inferred along axis mantle temperature variation and classification as an end-member example make the SWIR an excellent location to study the effect of mantle temperature and/or magma supply variability on abyssal hill morphology.

[5] Temporal variability of magma supply is also thought to affect the volume of volcanic crust produced [e.g., *Behn and Ito*, 2008; *Cannat et al.*, 2008, 2006]. Reduction of crustal thickness relative to the rigid upper mantle will strengthen the lithosphere and should result in larger abyssal hills [*Behn and Ito*, 2008; *Shaw and Lin*, 1996]. In addition, reduced sub-axial magma supply in the deep, melt-poor part of the SWIR may result in focused upwelling to produce a patchwork of locally enhanced amounts of crust [*Bown and White*, 1994; *Sauter et al.*, 2011a] juxtaposed with areas of little or no volcanic crust [*Cannat et al.*, 2006]. Temporal variation of the accretion process within the context of a cool mantle temperature regime with reduced melt production is probably the principal cause for the formation of areas of lithosphere with very thin or no volcanic crustal component in this region [*Cannat et al.*, 2006, 2008]. The eastern SWIR displays the largest known expanses of seafloor with little or no volcanic upper crustal layer, also referred to as smooth seafloor [*Cannat et al.*, 2006]. The non-volcanic nature of these areas of seafloor is confirmed by deep-tow sonar data
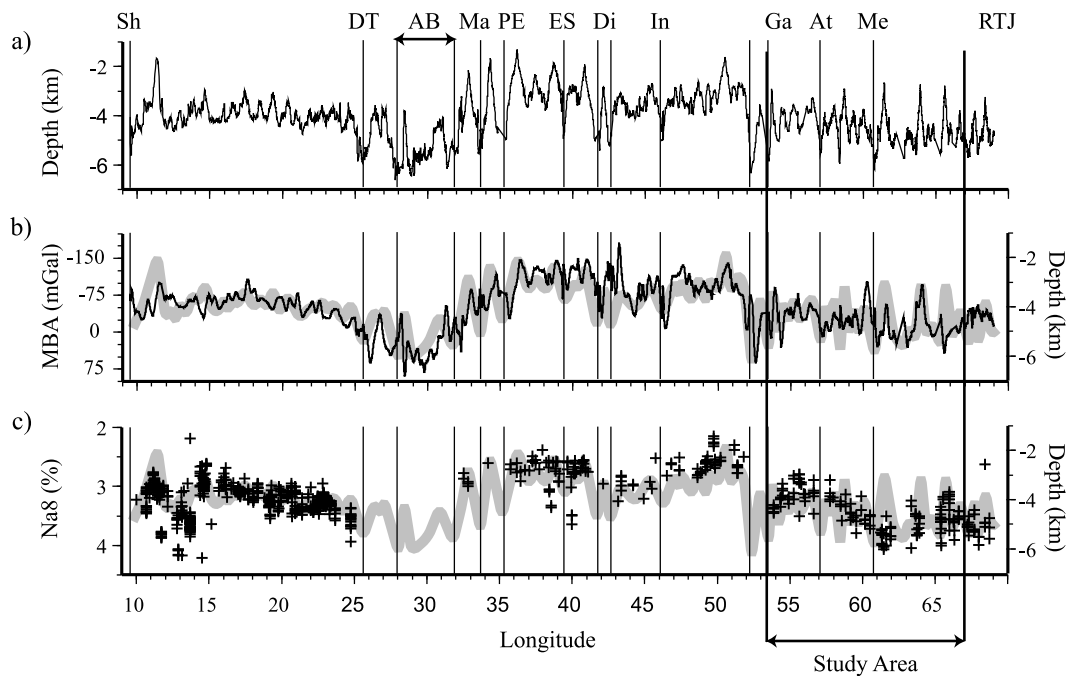
Figure 2. SWIR along-axis profiles from *Sauter and Cannat* [2010]: (a) depth [*Dick et al.*, 2003; *Grindlay et al.*, 1998; *Munschy and Schlich*, 1990; *Patriat et al.*, 1997; *Sauter et al.*, 2001, 2009], (b) mantle Bouguer anomaly [*Georgen et al.*, 2001], and (c) Na8.0 composition of dredged basalt glasses [*Cannat et al.*, 2008; *Sauter et al.*, 2009; *Standish et al.*, 2008] (subscript 8.0 refers to values corrected for low-pressure fractionation to a common MgO content of 8 wt%, as described by *Klein and Langmuir* [1987]). The thick gray line in Figures 2b and 2c represents the smoothed axial depth profile for comparison Sh: Shaka TF; DT: Du Toit TF; AB: Andrew Bain TF; Ma: Marion TF; PE: Prince Edward TF; ES: Eric Simpson TF; Di: Discovery I and II TFs; In: Indomed TF; Ga: Gallieni and Gazelle TFs; Me: Melville TF; RTJ: Rodrigues Triple Junction.

[*Sauter et al.*, 2004] and by the abundance of serpentinized mantle-derived peridotites dredged from the axial valley [*Seyler et al.*, 2003] and on the flanks [*Sauter et al.*, 2011b] with only minor, occasional basalts and gabbros.

[6] The multibeam bathymetry and gravity data compiled along the SWIR from 54°E to 67°E (Figure 1) provides a unique opportunity to analyze abyssal hill characteristics along flow line corridors that traverse a change in spreading rate from slow to ultraslow. In addition, it allows us to determine whether the progressive west-to-east cooling of inferred mantle temperature is reflected in abyssal hill morphology and whether abyssal hill morphology varies from volcanic to non-volcanic seafloor. Based upon our findings, we discuss the implications of abyssal hill morphology in relation to spreading rate change, magma supply and lithosphere strength.

2. Data and Methods

[7] We compiled and merged multibeam bathymetric and gravity data from several French, U.S.,

and Japanese surveys and transits of the SWIR between 54°E and 67°E [*Baines et al.*, 2007; *Cannat et al.*, 2003, 2006; *Dick et al.*, 1991; *Fujimoto et al.*, 1999; *Hosford et al.*, 2003; *Mendel et al.*, 1997, 2003; *Munschy and Schlich*, 1990; *Patriat et al.*, 1997; *Sauter et al.*, 2001, 2002, 2011a, 2011b]. These bathymetry data have a horizontal resolution of 1% to 2% of seafloor depth and thus do not image seafloor structures less than 100 m to 120 m across. Taking into account this resolution limit, the merged data set was gridded at 0.15 km node spacing, which is sufficient to derive basic characteristics of the seafloor morphology. Seismic data within the region indicates negligible sediment thickness [*Sauter et al.*, 2011a].

[8] We used the stochastic modeling procedure of *Goff and Jordan* [1988, 1989] to analyze the statistical properties of abyssal hill morphology on the flanks of the SWIR. Subset areas of multibeam coverage, referred to as "boxes," were utilized for analysis (Figure 1). The boxes were chosen so as to exclude non-abyssal hill features such as fracture or discordant zones and seamounts. The boxes are polygonal, with their longest, straight, parallel

or sub-parallel sides aligned with the spreading direction or flow line. Each box extends for distances of ∼30 to ∼110 km along the flow line trend, spanning age intervals of ∼3–5 Myr. The bathymetry data within the boxes are resampled onto a new grid aligned with the flow line orientation as determined by *Patriat et al.* [2008], with rows representing the along-flow line direction and columns the across-flow line direction. Columns are detrended up to order 3, depending on the macro-scale bathymetry. After detrending, stochastic parameters are estimated with a weighted, least squares inversion [*Goff and Jordan*, 1988, 1989]. Derived parameters include the root mean square (RMS) height, which is the average variation of depths with respect to the regional depth trend, characteristic length and width, abyssal hill strike or azimuth, and fractal dimension.

[9] In this study we focus principally on (1) the RMS height, (2) the lineament azimuth and (3) the characteristic width defined as the width of the covariant function perpendicular to the azimuth [*Goff and Jordan*, 1988]. Although statistically robust, the RMS height underestimates the actual relief of abyssal hills [*Small*, 1998]. We therefore include an analysis of the amplitude of relief, defined as the difference between the minimum and maximum values of the bathymetric data [*Small*, 1998], to provide an additional characterization of abyssal hill morphology. Relief amplitude is calculated from gridded bathymetry corrected for the effect of thermal subsidence. The thermal subsidence correction was calculated from a smoothed surface age grid derived from isochrons of *Patriat et al.* [2008], *Sauter et al.* [2008], and *Lemaux et al.* [2002] using the empirical depth (D) versus age (t) curve of *Parsons and Sclater* [1977], $D_{(t)} = 350 \, t^{1/2} + D_{(t = 0)}$, where $D_{(t = 0)}$ is the depth of the zero-age ridge crest.

[10] We derived mean values of the mantle Bouguer anomaly (MBA) within each of the boxes from grids calculated by *Sauter et al.* [2011a] using an assumed crustal thickness of 5 km with a constant density of 2700 kg/m³. Each box spans a different range of seafloor ages and therefore the degree of thermal subsidence varies from box to box. In order to obtain comparable depth and mean MBA values, we sub-sampled within ultraslow boxes for the common age range of 8–13 Ma and within slow boxes for ages 26–31 Ma.

[11] Of the 36 boxes analyzed, 30 extend along extensional flow lines at or near segment centers, and six are located within zones of non-volcanic

seafloor (Figure 1). Non-volcanic seafloor at the SWIR has only been identified to the east of 61°E, typically in or near discordant zones [*Cannat et al.*, 2008]. Several volcanic ultraslow boxes are also located in this area. Nine of the 30 segment center boxes contain seafloor generated at the rate of 30 mm/yr, between C13n.y and C8n.o [*Patriat et al.*, 2008]. The other 21 segment center boxes contain seafloor generated at 15 mm/yr, between C6n.o and C3An.y [*Patriat et al.*, 2008]. Every effort was made to select boxes with a full range of well-developed abyssal hill morphologies and to avoid inside and outside corner relief. Relief associated with the axial valley and ridge mountains was excluded by selecting seafloor older than C3An.y. We also avoided corrugated surfaces associated with mega-mullions structures as identified by *Baines et al.* [2003], *Cannat et al.* [2006, 2009], *Dick et al.* [1991], *Searle et al.* [2003], and *Searle and Bralee* [2007].

[12] One box to the west of Atlantis II FZ has anomalously large RMS height and characteristic width values. It is located within a segment bounded to the west by what was once a 45-km-long transform fault at 56°30′E. This transform fault evolved into an 11-km offset non-transform discontinuity when spreading rate decreased [*Baines et al.*, 2007], a change in plate boundary geometry that may have disrupted abyssal hill organization and produced anomalously high estimations of abyssal hill statistical parameters. This anomalous result illustrates the importance of box position to obtaining representative results from the analysis.

[13] In order to examine abyssal hill morphology within the ensemble of the compiled bathymetry data we filtered the bathymetry grid to isolate intermediate wavelength bathymetric features that correspond to abyssal hill morphology (Figure 3). Considering the range of characteristic abyssal hill width of ∼6.4 km to ∼8.5 km, the upper limit of the filter was set at wavelengths 15 km. The lower limit was set at wavelengths of <2 km, corresponding to volcanic edifices and small-scale fault textures.

3. Results

[14] Our interest lies in the variability of abyssal hill character with spreading rate change, with mantle temperature variation and with the presence or absence of volcanic crust. We therefore present our results within the context of variability along flow lines, variability parallel to the axis (i.e., with
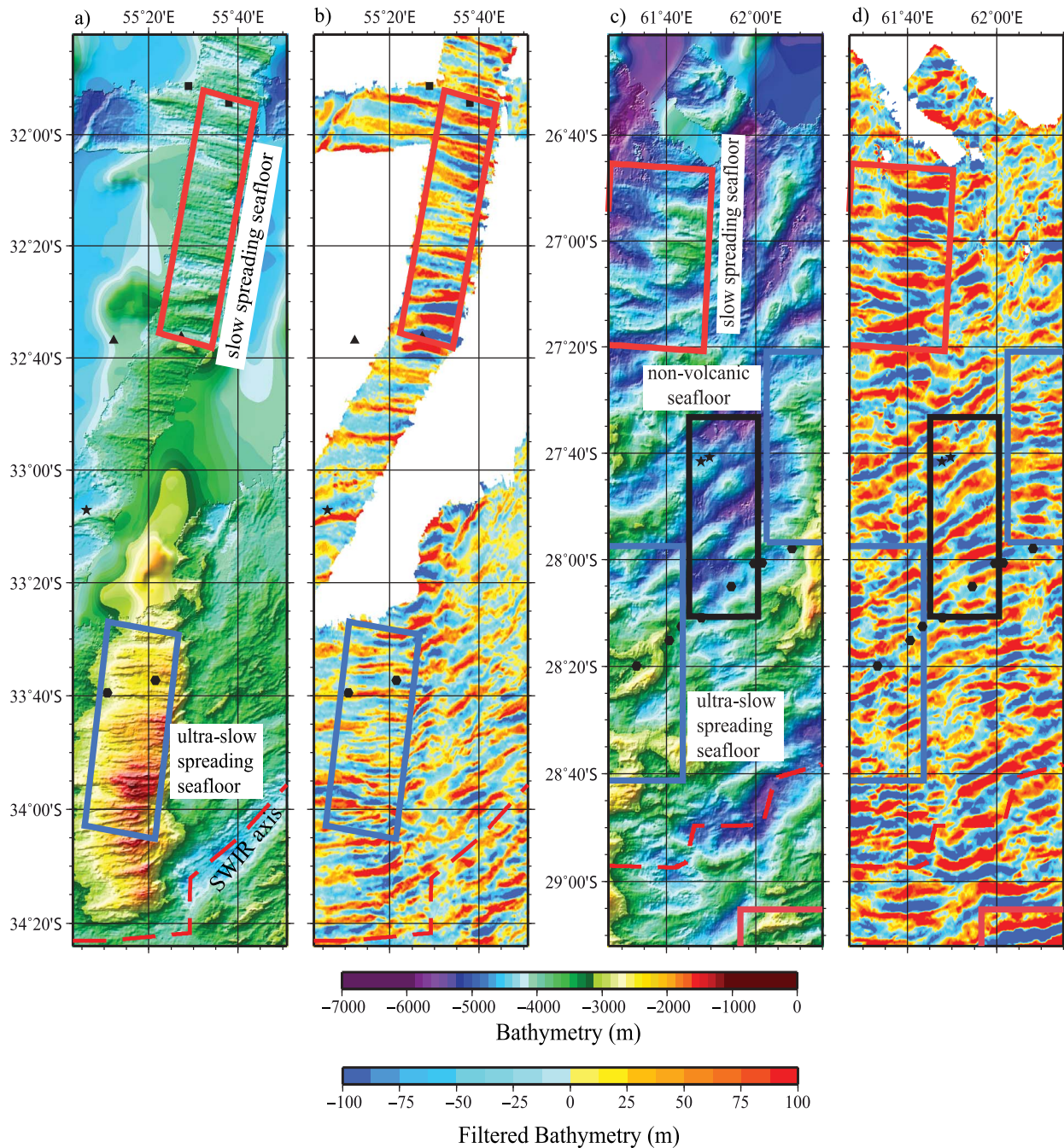
Figure 3. Extracted examples of boxes of bathymetry and intermediate wavelength filtered bathymetry used for analysis: slow segment center (red), ultraslow volcanic segment center (blue), and non-volcanic seafloor (black); (a) bathymetry located between Gallieni and Atlantis II FZ; (b) filtered bathymetry shown in Figure 3a; (c) bathymetry located to the east of Melville FZ; (d) filtered bathymetry shown in Figure 3c. In Figures 3b and 3d, intermediate wavelengths corresponding to the abyssal hills have been retained while wavelengths corresponding to the volcanic texture (<2 km) and to the regional trend (>15 km) were removed. Magnetic anomaly identifications: A6 (stars), A8 (triangles), and A13 (squares).

longitude), and volcanic or non-volcanic lithosphere. The calculated mean values of abyssal hill parameter estimates and proportional error estimates for each type of seafloor morphology analyzed are summarized in Table 1. Results of the statistical analysis, relief amplitude calculation, mean depth, and mean MBA values within each box appear graphically in Figure 4.

Table 1. Mean Abyssal Hill Characteristics With 1-sigma Errors

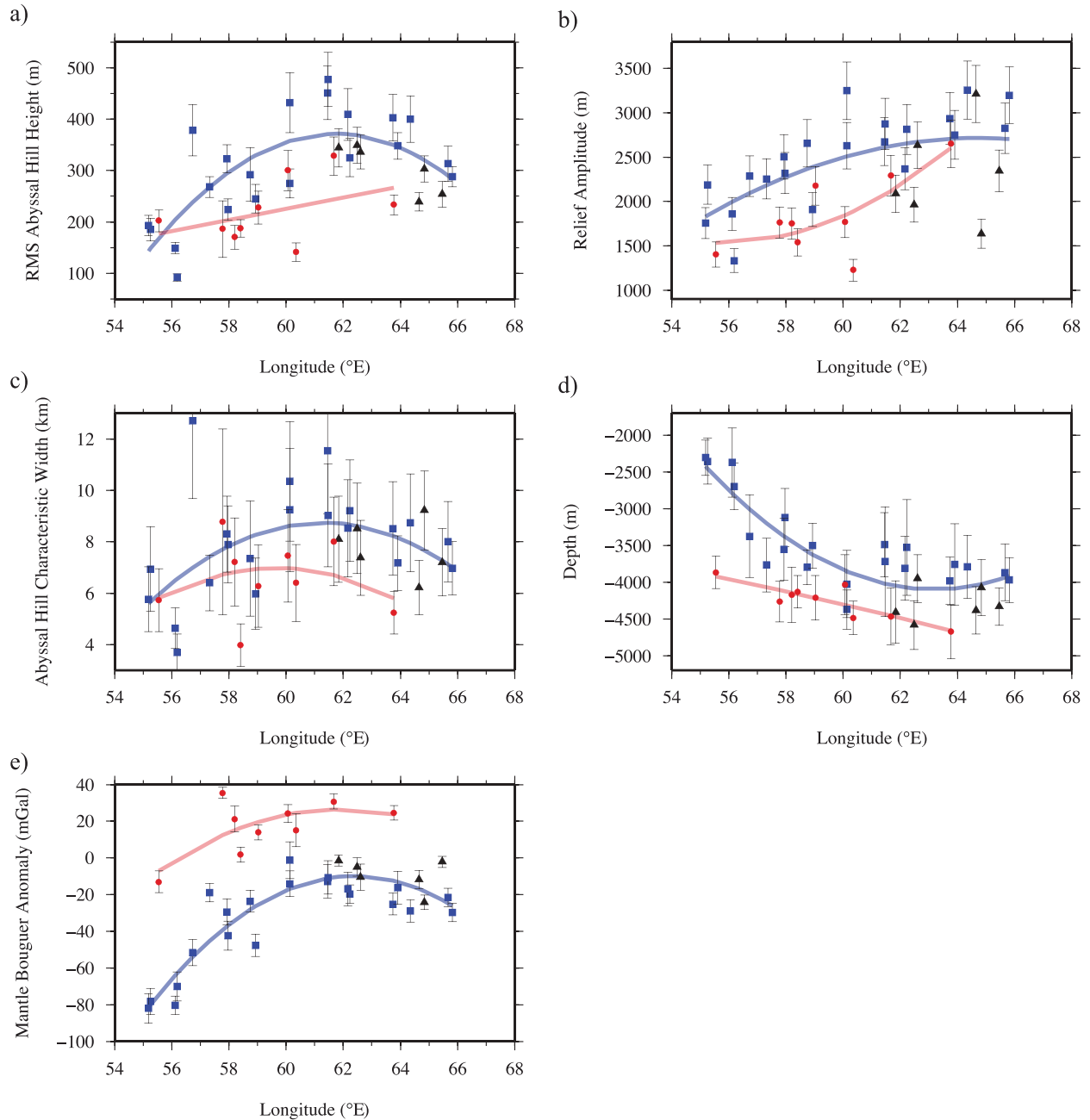| Seafloor Type	Full Rate (mm/yr)	RMS Height (m)	Characteristic Width (km)	Azimuth (deg)	Relief Amplitude (m)	Depth (m)	MBA (mgal)
Slow	30	222 ± 22	6.4 ± 0.5	95 ± 4	1800 ± 159	4298 ± 273	17 ± 5
Ultraslow	15	298 ± 23	7.8 ± 0.5	83 ± 2	2507 ± 114	3455 ± 570	−34 ± 6
Ultraslow Volcanic 61–67°E	15	372 ± 23	8.5 ± 0.5	78 ± 4	2855 ± 267	3753 ± 173	−20 ± 2
Ultraslow Non-volcanic 61–67°E	15	304 ± 20	8.0 ± 0.4	61 ± 4	2314 ± 227	4393 ± 142	−9 ± 2

Figure 4. Abyssal hill characteristics with 1-sigma error bars plotted with longitude: (a) RMS height, m; (b) relief amplitude, m; (c) characteristic width, km; (d) mean depth, m; and (e) MBA values, mGal. Red circles represent slow seafloor, blue squares represent values for ultraslow volcanic seafloor, and black triangles represent non-volcanic ultraslow seafloor.

3.1. Along-Flow Line Variation: From Slow to Ultraslow

[15] RMS abyssal hill height mean value for all ultraslow spreading boxes (298 ± 23 m) is significantly larger than that for slow spreading boxes (222 ± 22 m). The two populations are clearly distinct in Figure 4a. Mean abyssal hill relief amplitude variation (Figure 4b) is consistent with that of the RMS height, indicating coherent estimates of abyssal hill height. The mean value of characteristic abyssal hill width for ultraslow spreading boxes (7.8 ± 0.5 km) is larger than that for slow spreading boxes (6.4 ± 0.5 km) (Figure 4c). The difference between the two populations is 1.4 km, while the standard deviation of both populations is 0.5 km. Regression trends for the two characteristic width populations indicate that they are significantly distinct. Mean azimuth values (Table 1) indicate a ~12° change in the orientation of abyssal hills following the transition from slow to ultraslow spreading, a figure consistent with the kinematic reconstruction of *Patriat et al.* [2008].

3.2. Variation West-to-East: Decreasing Inferred Mantle Temperature

[16] There is marked and correlated variation in abyssal hill morphology, seafloor depth and MBA values west-to-east (Figure 4). Ultraslow abyssal hills generally have greater RMS heights and relief amplitude at a given longitude. From 54°E to 61°E, both slow and ultraslow abyssal hill populations display a significant eastward increase in RMS height. East of 61°E, ultraslow RMS abyssal hill height values decrease slightly, approaching the mean. Relief amplitude of both slow and ultraslow populations increases steadily with longitude.

[17] The characteristic abyssal hill width increases from 54°E to 61°E with a significant difference between the slow and ultraslow populations. When RMS heights versus characteristic width for all boxes is plotted (Figure 5a), the correlation coefficient is robust at +0.72, resolvable at >0 at 99.9% confidence (T-test). A correlation coefficient of +0.74 is found for mean MBA value and RMS abyssal hill height (Figure 5b). As there are only 9 boxes selected on slow spreading seafloor, the correlation between RMS abyssal hill height, characteristic abyssal hill width and MBA for this population is indeterminate.

[18] Depth values for both slow and ultraslow boxes increase from 54°E to 61°E (Figures 4d and 4e). East of 61°E, ultraslow depth remains approximately constant. MBA values for slow and ultraslow boxes increase steadily from 54°E to 61°E. MBA value regression trend slopes are similar for slow and ultraslow boxes. MBA values for ultraslow boxes decrease slightly east of 61°E.

3.3. Volcanic and Non-volcanic Lithosphere

[19] Within the study area, non-volcanic seafloor was detected only east of 61°E (Figure 1). The six boxes containing non-volcanic seafloor are located on ultraslow seafloor. Another 11 boxes located east of 61°E contain volcanic seafloor, two on slow seafloor and nine on ultraslow seafloor (Figure 1). The mean RMS abyssal hill height for boxes containing volcanic lithosphere is 372 ± 23 m (Table 1). The mean RMS height for non-volcanic boxes is significantly smaller at 304 ± 20 m (Table 1). The non-volcanic boxes display RMS height values that are intermediate between those of slow and ultraslow boxes while the non-volcanic relief amplitude tends to be lower than both slow and ultraslow volcanic boxes within the same range of longitude. Mean characteristic widths of volcanic and non-volcanic boxes are 8.5 ± 0.5 km and 8.0 ± 0.4 km, respectively.

[20] Depth values for ultraslow non-volcanic boxes are ~700 m deeper than ultraslow volcanic boxes east of 61°E. MBA values of ultraslow non-volcanic boxes are greater than those of ultraslow volcanic boxes east of 61°E, with mean values of −9 ± 2 mGal and −20 ± 2 mGal, respectively (Table 1). Non-volcanic abyssal hill mean azimuth is 61° ± 4° while volcanic abyssal hill mean azimuth is 78° ± 4° (Table 1), indicating that non-volcanic abyssal hill azimuths are significantly more oblique to spreading direction.

[21] The intermediate wavelength filtered bathymetry reveals the lateral continuity of individual abyssal hills that extend continuously across non-volcanic and volcanic seafloor (Figure 3). The non-volcanic seafloor abyssal hill azimuths align with magnetic anomalies just as they do for volcanic seafloor abyssal hills, but with a difference in mean azimuth of ~17°.

4. Discussion

[22] The results of our statistical analysis of seafloor bathymetry on the flanks of the SWIR provide internally consistent and globally comparable
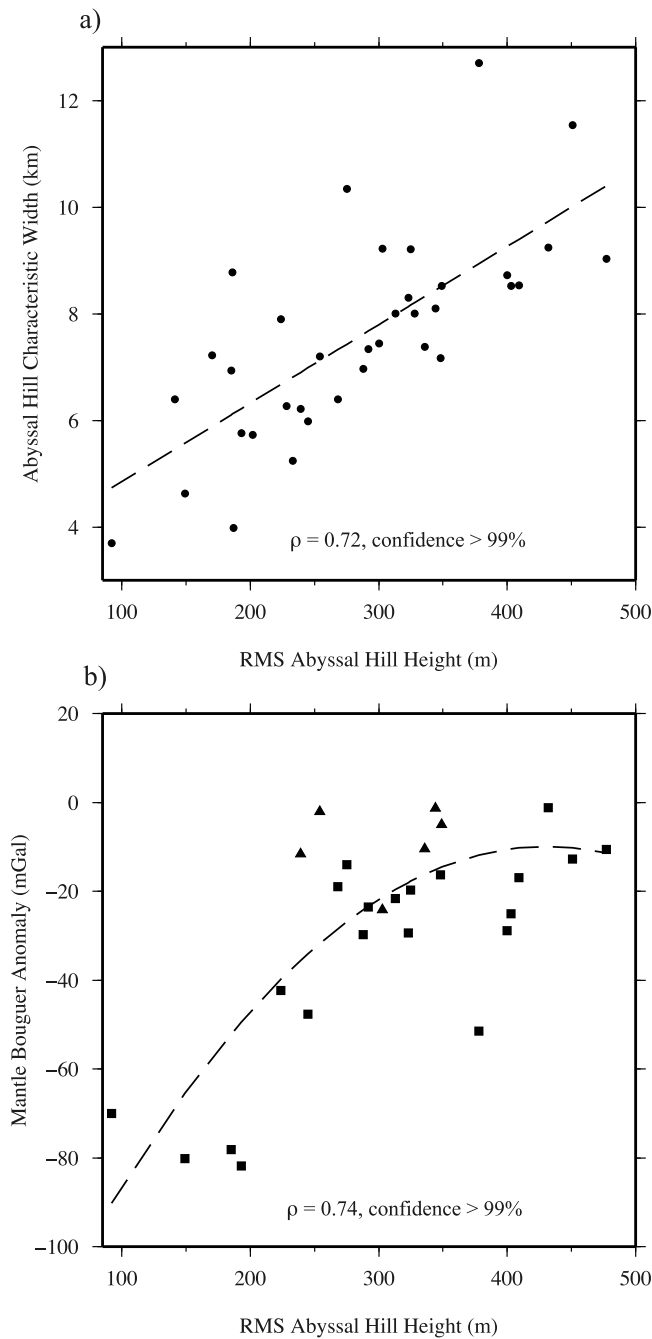
Figure 5. Correlations between (a) RMS abyssal hill height and characteristic abyssal hill width for all boxes and (b) RMS abyssal hill height and mantle Bouguer anomaly for ultraslow spreading boxes; squares represent values for ultraslow volcanic seafloor and triangles represent ultraslow non-volcanic seafloor.

characterization of abyssal hill morphology at an ultraslow spreading ridge. Based upon this analysis we determine the variability of abyssal hill morphology resulting from a change in spreading rate from slow to ultraslow, a regional gradient in sub-axial melt supply and/or mantle temperature, and the presence or absence of volcanic crust.

Combining this analysis with inferred crustal thickness derived from MBA values, we discuss variation of lithosphere rheology with decreasing mantle temperature as a probable governing factor in the formation and evolution of abyssal hills. We are also able to determine morphologic parameters of abyssal hills generated at ultraslow spreading rates.

4.1. Effect of Spreading Rate Change From Slow to Ultraslow on Abyssal Hill Morphology

[23] The significant difference in the RMS abyssal hill height, relief amplitude, and characteristic width values for slow and ultraslow seafloor, both overall mean values and values for individual boxes at a given longitude, is a clear indicator that the spreading rate change from 30 mm/yr to 15 mm/yr had a profound effect on abyssal hill morphology. This inference is supported by the close correlation between abyssal hill characteristic width and RMS height (Figure 5a). The significant increase in RMS abyssal hill height, characteristic width, and relief amplitude with decreasing spreading rate at this relatively cool, magma-poor region of the mid-ocean ridge system, confirms that faulting is a dominant contributing factor to abyssal hill relief at slower spreading rates [e.g., *Escartín and Lin*, 1998; *MacDonald and Luyendyk*, 1977; *Neumann and Forsyth*, 1995; *Searle et al.*, 1998; *Shaw*, 1992; *Shaw and Lin*, 1993]. The increase in abyssal hill height is consistent with the notions that elastic lithosphere generated at slower spreading rates is relatively thicker [e.g., *Phipps Morgan and Chen*, 1993; *Shaw and Lin*, 1996] and is thus able to sustain greater relief through faulting and flexure [*Malinverno*, 1993; *Shaw and Lin*, 1996]. The similar RMBA values for ultraslow seafloor compared to slow seafloor [*Cannat et al.*, 2006; *Sauter et al.*, 2011a] suggests that either the crustal thickness does not change or that it thins and is compensated by a corresponding change in mantle density due to enhanced cooling as a result of the spreading rate change. If the thickness of the crustal component of the lithosphere does not change, this suggests that the change in lithosphere rheology that produced greater abyssal hill relief occurred in the mantle portion of the lithosphere.

[24] The spreading rate change at 24 Ma was accompanied by a 13° change in spreading direction [*Patriat et al.*, 2008]. The corresponding 12° change in abyssal hill azimuth for volcanic seafloor is remarkably similar, suggesting that the far field stresses governing plate motion may also influence abyssal hill orientation.

4.2. Effect of Regional Spatial Variation of Inferred Mantle Temperature and Magma Supply on Abyssal Hill Morphology

[25] The pronounced variation of abyssal hill parameters with longitude for both slow and ultraslow seafloor (Figure 4) indicates that spreading rate is not the sole controlling factor. From 54°E to 61°E on the flanks of the SWIR, RMS height, relief amplitude, characteristic width, depth, and MBA values all increase steadily for both slow and ultraslow seafloor. Similar regional gravity and bathymetric variations were found along the ridge axis (Figure 2) [*Cannat et al.*, 1999; *Sauter and Cannat*, 2010]. These findings are further supported by the steady west-to-east increase of $Na_{8.0}$ content and a corresponding decrease in the content of $Fe_{8.0}$ in basalts dredged from the axial valley [*Meyzen et al.*, 2003]. These results have been interpreted as a reduction of the degree of partial melting beneath the axis west-to-east due to progressively cooler sub-axial mantle temperature [e.g., *Cannat et al.*, 2008; *Sauter et al.*, 2011a]. Since elastic strength of the lithosphere is dependent upon thermal structure [*McNutt*, 1984], the eastward decrease in mantle temperature should produce increasing lithosphere thickness and strength west-to-east. Progressively increasing RMS height, relief amplitude, characteristic width, and depth values correlate well with the interpretation of progressively thicker, stronger lithosphere west-to-east (Figure 4). The west-to-east increase in RMS height also correlates with increasing MBA values for ultraslow (Figure 5b), indicating progressively thinner crust and/or cooler mantle temperatures; either case should produce progressive strengthening of the lithospheric mantle. Increasing abyssal hill height with decreasing crustal thickness and/or cooler mantle temperatures lends further support to the notion that abyssal hill RMS height and characteristic width are primarily controlled by the strength of the mantle component of the lithosphere.

4.3. Effect of Small-Scale Variation of Magma Supply on Abyssal Hill Morphology

[26] It is clear in Figure 4 that the character of the flanks of the SWIR east of 61°E breaks from the regional trends of abyssal hill morphology, depth, and inferred crustal thickness. Seafloor texture in this region is also distinctive with juxtaposed areas of volcanic and non-volcanic seafloor. This break has been linked to the inferred regional trend in sub-axial mantle temperature [*Cannat et al.*, 2008; *Sauter et al.*, 2011a]. The regional decrease in mantle temperature may result in focused upwelling east of 61°E, limiting delivery of melt to the surface [e.g., *Cannat et al.*, 2008; *Sauter et al.*, 2011a] to produce patches of volcanic and non-volcanic seafloor. If patches of volcanic and non-volcanic seafloor at the SWIR are indicators of reduced melt supply and temporal variation of accretion as has

been suggested [e.g., *Cannat et al.*, 2006; *Sauter and Cannat*, 2010], then this variation appears to occur on the scale of tens of kilometers and millions of years. High MBA values and abundant serpentinized mantle-derived peridotites, with only minor basalts and gabbros dredged from non-volcanic seafloor [*Sauter and Cannat*, 2010; *Seyler et al.*, 2003] are consistent with reduced magma supply compared to adjacent volcanic seafloor where basalts and gabbros are more abundant [*Sauter et al.*, 2011b; *Seyler et al.*, 2003]. Within areas of volcanic seafloor, produced by focused upwelling, the magmatic component of the lithosphere is thought to be comparatively greater [*Bown and White*, 1994; *Cannat et al.*, 2008] as indicated by mean MBA values that are ~10 mGal lower than for non-volcanic seafloor. Thus, these two types of seafloor present evidence of contrasting composition and rheology. Lithosphere should be thinner, warmer and weaker where upwelling is focused and thicker, colder and stronger where upwelling is reduced or absent [*Behn et al.*, 2006; *Cannat et al.*, 2008]. However, the mean value of RMS height of abyssal hills in volcanic seafloor is ~70 m greater than that for non-volcanic seafloor from 61°E to 67°E. Relief amplitude of volcanic seafloor is also greater than for non-volcanic seafloor. This apparent contradiction is explained by considering the differences in both rheology and tectonic deformation style of volcanic and non-volcanic seafloor. The volcanic seafloor composition is inferred to include the full complement of oceanic lithosphere components (i.e., volcanic and intrusive crust overlying upper mantle) [*Cannat et al.*, 2008] that tends to accommodate extension by high-angle normal faults. The non-volcanic seafloor is inferred to consist largely of serpentinzed peridotites above unaltered mantle that may contain trapped melt [*Cannat et al.*, 2009] in which the formation of low-angle detachment faults is more common [*Sauter et al.*, 2011b]. Low-angle detachment faults generally produce less relief, and thus lower abyssal hills, than high-angle normal faults. The intermediate wavelength (2 km $\langle \lambda \rangle$ 15 km) features revealed in the filtered bathymetry (Figure 3) clearly show the continuity of individual abyssal hills across volcanic and non-volcanic seafloor, suggesting that the low-angle detachments bounding abyssal hills in non-volcanic seafloor may extend into and interconnect with the higher angle faults in volcanic terrains. The fact that abyssal hills extend continuously across volcanic and non-volcanic seafloor with little variation in width at this ultraslow ridge is a strong indication that their

morphology is controlled by faulting rather than by magmatic processes. It has been suggested that fault spacing that determines abyssal hill width may be controlled by axial valley morphology [*Goff et al.*, 1997; *Malinverno and Gilbert*, 1989; *Shaw*, 1992; *Shaw and Lin*, 1993]. The constant presence of a deep axial valley along the entire length of the SWIR within the study area may play a role in limiting the variation in abyssal hill width in volcanic and non-volcanic ultraslow seafloor.

[27] East of 61°E there are tens of kilometers long sections of the ridge oriented oblique to the spreading direction and associated with similarly oblique abyssal hill fabric in non-volcanic seafloor on the adjacent flanks. The mean azimuth of non-volcanic abyssal hills east of 61°E at the SWIR is ~32° oblique to the N3°E spreading direction while volcanic abyssal hills are ~15° oblique, suggesting a response to far field stress that varies with contrasting lithosphere rheology and tectonic deformation style. Another contributing factor to the obliquity of abyssal hills here may be the configuration of the sub-axial zone of mantle upwelling: alignment of magnetic anomalies with abyssal hill azimuth suggests that the zone of upwelling is probably also oblique to the spreading direction.

4.4. Ultraslow Spreading Abyssal Hill Characterization

[28] Comparison of the results of our analysis of abyssal hill morphology with similar analyses conducted at slow and intermediate spreading ridges is presented in Table 2. There is currently no comparable analysis at another ultraslow spreading ridge. RMS seafloor roughness at the ultraslow Arctic ridges, are estimated as ranging from 450 m to 584 m using the method of *Malinverno* [1991] on individual seismic profiles [*Ehlers and Jokat*, 2009; *Weigelt and Jokat*, 2001]. These values may not be comparable to our statistical analysis at the SWIR as they are estimated from only two profiles of seismically determined basement, one of which crosses the ridge, in a region where sediment thickness is as great as 3200 m. *Ehlers and Jokat* [2009] noted that seafloor roughness values from a variety of ridges with the same spreading rate scatter around the best fit seafloor roughness versus spreading rate curve calculated by *Malinverno* [1991] [*Ehlers and Jokat*, 2009, Figure 6]. This may be due to mantle temperature variability since there is no significant variation of spreading to account for it. RMS height values (~222 m) for slow (30 mm/yr full rate) seafloor at the SWIR

Table 2. Abyssal Hill RMS Height and Mean Characteristic Width for Slow and Ultraslow Spreading Ridges With 1-sigma Errors[a]

Ridge	Full Spreading Rate (mm/yr)	RMS Height (m)	Characteristic Width (km)
SWIR ultraslow	15	297 ± 23	7.8 ± 0.5
SWIR slow	30	222 ± 22	6.4 ± 0.5
MAR north [Goff et al., 1995]	26	236 ± 8	8.2 ± 0.3
MAR south [Neumann and Forsyth, 1995]	32	222	6.0
MAR south [Goff, 1991]	36	201 ± 18	5.7 ± 0.6
SEIR axial high near St Paul and Amsterdam hotspot [Goff et al., 1997; Cochran et al., 1997]	72	62 ± 2	1.8 ± 0.1
SEIR intermediate axial valley morphology [Goff et al., 1997; Cochran et al., 1997]	~74	97 ± 3	3.1 ± 0.1
SEIR axial valley close to ADD [Goff et al., 1997; Cochran et al., 1997]	76	170 ± 7	4.0 ± 0.3

[a]Error estimates are not available from *Neumann and Forsyth* [1995].

are similar to those estimated using the same method on the Mid-Atlantic Ridge (MAR) (∼220–240 m) [*Goff et al.*, 1995; *Neumann and Forsyth*, 1995] (Table 2). As spreading rate increases from north to south along the MAR from 26 mm/yr to 36 mm/yr, the RMS height decreases from ∼236 m to ∼201 m, respectively. At intermediate spreading rates of 72–76 mm/yr at the Southeast Indian Ridge (SEIR), RMS heights range from ∼170 m near the Australian-Antarctic Discordance (AAD) to ∼62 m near the St Paul and Amsterdam hot spot [*Cochran et al.*, 1997]. This rather broad range of RMS height occurs along the SEIR from the AAD to the St Paul and Amsterdam hot spot where spreading rate varies only slightly, but a thermal gradient within the upper mantle has been correlated with variation of lithosphere rheology similar to that inferred at the SWIR [*Sempéré et al.*, 1997].

[29] Based upon our findings and comparison with other slow to intermediate spreading ridges, it is possible to characterize mean ultraslow spreading generate abyssal hill RMS heights in volcanic seafloor as ranging from ∼275 m to ∼325 m or possibly greater. In areas of ultraslow seafloor where patches of volcanic and non-volcanic terrain occur, the variability of RMS height resulting from differences in lithosphere rheology and tectonic deformation style prevent characterization of abyssal hill height. Abyssal hill widths for ultraslow seafloor range from 3.7 km to 12.7 km, averaging ∼8 km, and do not vary significantly from volcanic to non-volcanic seafloor.

5. Conclusions

[30] This study characterizes abyssal hill morphology on the flanks of the Southwest Indian Ridge from 54°E to 67°E using the statistical analysis method of *Goff and Jordan* [1988, 1989] on compiled multibeam bathymetry data. The analysis is combined with compiled gravity data from the same zone to provide inferred crustal thickness estimates. The region encompassed by the compiled data includes a spreading rate change from slow to ultraslow at ∼24 Ma, a significant inferred variation in sub-axis mantle temperature, and a patchwork of volcanic and non-volcanic seafloor. We draw the following conclusions:

[31] RMS height and characteristic width of abyssal hills increased when the full spreading rate changed from 30 mm/yr to 15 mm/yr. MBA values indicate that as a result of the spreading rate change the crustal thickness either remained constant or thinned with a corresponding compensating change in mantle density. We suggest that the former is the correct interpretation, although both interpretations call for strengthening of the mantle lithosphere. We, thus, conclude that greater abyssal hill relief of ultraslow seafloor is due to strengthening of the mantle portion of the lithosphere as a result of spreading rate change.

[32] From 54°E to 61°E the west-to-east increase in depth coupled with the results of geochemical sampling and analysis correlated with increasing MBA values are indicative of progressively decreasing mantle temperature, causing eastward decrease of melt supply to the axis and increasingly thicker, stronger lithosphere. The corresponding increase of RMS abyssal hill heights for both slow and ultraslow seafloor lead us to conclude that abyssal hill height is primarily controlled by the strength of the mantle component of the lithosphere rather than spreading rate and may, thus, be fundamentally linked to mantle temperature.

[33] The occurrence of juxtaposed patches of volcanic and non-volcanic seafloor in the region east of 61°E is probably due to focused mantle upwelling within this region of cooler mantle temperatures and overall reduced melt supply. We found that not only do abyssal hills occur in non-volcanic seafloor, but that individual abyssal hill structures extend continuously from non-volcanic seafloor into volcanic seafloor changing azimuth trend from near-orthogonal to moderately oblique to spreading direction as they do so. Contrasting lithosphere rheology and tectonic deformation style of volcanic and non-volcanic seafloor is probably responsible for comparatively lower RMS abyssal hill height for non-volcanic seafloor. Continuity of abyssal hills across volcanic and non-volcanic seafloor with little or no change in their width suggests that abyssal hill morphology is controlled by tectonic rather than magmatic processes.

[34] We propose a characteristic RMS height range of ~275 m to ~325 m or possible greater for abyssal hills in volcanic seafloor generated at ultraslow spreading rates and a characteristic average width of ~8 km. Based upon this study it is not possible to determine a characteristic RMS abyssal hill height for areas of non-volcanic seafloor due the variability of lithosphere rheology and tectonic style in these areas.

Acknowledgments

References

Baines, A. G., M. J. Cheadle, H. J. B. Dick, A. Hosford, A. Scheirer, B. E. John, N. J. Kusznir, and T. Matsumoto (2003), Mechanism for generating the anomalous uplift of oceanic core complexes: Atlantis Bank, Southwest Indian Ridge, *Geology*, *31*, 1105–1108, doi:10.1130/G19829.1.

Baines, A. G., M. J. Cheadle, H. J. B. Dick, A. Scheirer, B. E. John, N. J. Kusznir, and T. Matsumoto (2007), Evolution of the Southwest Indian Ridge from 55°45′E to 62°E: Changes in plate-boundary geometry since 26 Ma, *Geochem. Geophys. Geosyst.*, *8*, Q06022, doi:10.1029/2006GC001559.

Behn, M. D., and G. Ito (2008), Magmatic and tectonic extension at mid-ocean ridges: 1. Controls on fault characteristics, *Geochem. Geophys. Geosyst.*, *9*, Q08O10, doi:10.1029/2008GC001965.

Behn, M. D., W. R. Buck, and I. S. Sacks (2006), Topographic controls on dike injection in volcanic rift zones, *Earth Planet. Sci. Lett.*, *246*, 188–196, doi:10.1016/j.epsl.2006.04.005.

Bown, J. W., and R. S. White (1994), Variation with spreading rate of oceanic crustal thickness and geochemistry, *Earth Planet. Sci. Lett.*, *121*, 435–449, doi:10.1016/0012-821X(94)90082-5.

Buck, W. R., and A. N. B. Poliakov (1998), Abyssal hills formed by stretching oceanic lithosphere, *Nature*, *392*, 272–275, doi:10.1038/32636.

Buck, W. R., S. Carbotte, and C. Mutter (1997), Controls on extrusion at mid-ocean ridges, *Geology*, *25*, 935–938, doi:10.1130/0091-7613(1997)025<0935:COEAMO>2.3.CO;2.

Buck, W. R., L. L. Lavier, and A. N. B. Poliakov (2005), Modes of faulting at mid-ocean ridges, *Nature*, *434*, 719–723, doi:10.1038/nature03358.

Cannat, M., C. Rommevaux-Jestin, D. Sauter, C. Deplus, and V. Mendel (1999), Formation of the axial relief at the very slow spreading Southwest Indian Ridge (49°–69°E), *J. Geophys. Res.*, *104*, 22,825–22,843, doi:10.1029/1999JB900195.

Cannat, M., C. Rommevaux-Jestin, and H. Fujomoto (2003), Melt suppluy variations to a magma-poor ultra-slow spreading ridge (Southwest Indian Ridge 61° to 69°E), *Geochem. Geophys. Geosyst.*, *4*(8), 9104, doi:10.1029/2002GC000480.

Cannat, M., D. Sauter, V. Mendel, E. Ruellan, K. Okino, J. Escartín, V. Combier, and M. Baala (2006), Modes of seafloor generation at a melt-poor ultraslow-spreading ridge, *Geology*, *34*, 605–608, doi:10.1130/G22486.1.

Cannat, M., D. Sauter, A. Bezos, C. Meyzen, E. Humler, and M. Le Rigoleur (2008), Spreading rate, spreading obliquity, and melt supply at the ultraslow spreading Southwest Indian Ridge, *Geochem. Geophys. Geosyst.*, *9*, Q04002, doi:10.1029/2007GC001676.

Cannat, M., D. Sauter, J. Escartín, L. Lavier, and S. Picazo (2009), Oceanic corrugated surfaces and the strength of the axial lithosphere at slow spreading ridge, *Earth Planet. Sci. Lett.*, *288*, 174–183, doi:10.1016/j.epsl.2009.09.020.

Chen, Y., and W. J. Morgan (1990), A non-linear rheology model for mid-ocean ridge axis topography, *J. Geophys. Res.*, *95*, 17,583–17,604, doi:10.1029/JB095iB11p17583.

Cochran, J. R., J.-C. Sempéré, and the SEIR Scientific Team (1997), The Southeast Indian Ridge between 88°E and 120°E: Gravity anomalies and crustal accretion at intermediate spreading rates, *J. Geophys. Res.*, *102*(B7), 15,463–15,487, doi:10.1029/97JB00511.

Dick, H. J. B., H. Schouten, S. Meyer, D. G. Gallo, H. Bergh, R. Tyce, P. Patriat, K. T. M. Johnson, J. Snow, and A. Fischer (1991), Tectonic evolution of the Atlantis II Fracture Zone, *Proc. Ocean Drill. Program Sci. Results*, *118*, 359–398.

Dick, H. J. B., J. Lin, and H. Schouten (2003), An ultraslow class of spreading ridge, *Nature*, *426*, 405–412, doi:10.1038/nature02128.

Ehlers, B.-M., and W. Jokat (2009), Subsidence and crustal roughness of ultra-slow spreading ridges in the northern North Atlantic and the Arctic Ocean, *Geophys. J. Int.*, *177*, 451–462, doi:10.1111/j.1365-246X.2009.04078.x.

Escartín, J., and J. Lin (1998), Tectonic modification of axial crustal structure: Evidence from spectral analyses of residual gravity and bathymetry of the Mid-Atlantic Ridge flanks, *Earth Planet. Sci. Lett.*, *154*, 279–293, doi:10.1016/S0012-821X(97)00194-5.

Fujimoto, H., et al. (1999), First submersible investigations of mid-ocean ridges in the Indian Ocean, *InterRidge News*, *8*(1), 22–24.

Georgen, J., J. Lin, and H. J. B. Dick (2001), Evidence from gravity anomalies for interactions of the Marion and Bouvet hotspots with the Southwest Indian Ridge: Effects of transform offsets, *Earth Planet. Sci. Lett.*, *187*, 283–300, doi:10.1016/S0012-821X(01)00293-X.

Goff, J. A. (1991), A global and regional stochastic analysis of near-ridge abyssal hill morphology, *J. Geophys. Res.*, *96*, 21,713–21,737, doi:10.1029/91JB02275.

Goff, J. A. (1992), Quantitative characterization of abyssal hill morphology along flow lines in the Atlantic Ocean, *J. Geophys. Res.*, *97*, 9183–9202, doi:10.1029/92JB00602.

Goff, J. A., and T. Jordan (1988), Stochastic modeling of seafloor morphology: Inversion of SeaBeam data for second order statistics, *J. Geophys. Res.*, *93*, 13,589–13,608, doi:10.1029/JB093iB11p13589.

Goff, J. A., and T. H. Jordan (1989), Stochastic modeling of seafloor morphology: Resolution of topographic parameters by SeaBeam data, *IEEE J. Oceanic Eng.*, *14*, 326–337, doi:10.1109/48.35983.

Goff, J. A., A. Malinverno, D. J. Fornari, and J. R. Cochran (1993), Abyssal hill segmentation: Quantitative analysis of the East Pacific Rise flanks 7°S–9S, *J. Geophys. Res.*, *98*, 13,851–13,862, doi:10.1029/93JB01095.

Goff, J. A., B. E. Tucholke, J. Lin, G. E. Jaroslow, and M. C. Kleinrock (1995), Quantitative analysis of abyssal hills in the Atlantic Ocean: A correlation between axis crustal thickness and extensional faulting, *J. Geophys. Res.*, *100*, 22,509–22,522, doi:10.1029/95JB02510.

Goff, J. A., Y. Ma, A. Shah, J. R. Cochran, and J.-C. Sempéré (1997), Stochastic analysis of seafloor morphology on the flank of the Southeast Indian Ridge: The influence of ridge morphology on the formation of abyssal hills, *J. Geophys. Res.*, *102*, 15,521–15,534, doi:10.1029/97JB00781.

Grindlay, N. R., J. A. Madsen, C. Rommevaux-Jestin, and J. Sclater (1998), A different pattern of ridge segmentation and mantle Bouger gravity anomalies along the ultra-slow Southwest Indian Ridge (15°30′E to 25°E), *Earth Planet. Sci. Lett.*, *161*(1–4), 243–253, doi:10.1016/S0012-821X(98)00154-X.

Hosford, A., M. Tivey, T. Matsumoto, H. Dick, H. Schouten, and H. Kinoshita (2003), Crustal magnetization and accretion at the Southwest Indian Ridge near the Atlantis II Fracture Zone, 0–25 Ma, *J. Geophys. Res.*, *108*(B3), 2169, doi:10.1029/2001JB000604.

Klein, E. M., and C. H. Langmuir (1987), Global correlations of ocean ridge basalt chemistry with axial depth and crustal chemistry, *J. Geophys. Res.*, *92*, 8089–8115, doi:10.1029/JB092iB08p08089.

Lemaux, J., R. G. Gordon, and J.-Y. Royer (2002), Location of the Nubia-Somalia boundary along the Southwest Indian Ridge, *Geology*, *30*, 339–342, doi:10.1130/0091-7613(2002)030<0339:LOTNSB>2.0.CO;2.

Lin, J., and E. M. Parmentier (1989), Mechanism of lithospheric extension at mid-ocean ridges, *Geophys. J.*, *96*, 1–22, doi:10.1111/j.1365-246X.1989.tb05246.x.

Lin, J., and J. Phipps Morgan (1992), The spreading rate dependence of three-dimensional mid-ocean ridge gravity structure, *Geophys. Res. Lett.*, *19*, 13–15, doi:10.1029/91GL03041.

MacDonald, K. C., and B. P. Luyendyk (1977), Deep-tow studies of the structure of the Mid-Atlantic Ridge crest near lat 37°N, *Geol. Soc. Am. Bull.*, *88*, 621–636, doi:10.1130/0016-7606(1977)88<621:DSOTSO>2.0.CO;2.

MacDonald, K. C., P. J. Fox, R. T. Alexander, R. Pockalny, and P. Gente (1996), Volcanic growth faults and the origin of the Pacific abyssal hills, *Nature*, *380*, 125–129, doi:10.1038/380125a0.

Malinverno, A. (1991), Inverse square-root dependence of mid-ocean-ridge flank roughness on spreading rate, *Nature*, *352*, 58–60, doi:10.1038/352058a0.

Malinverno, A. (1993), Transition between a valley and a high at the axis of mid-ocean ridges, *Geology*, *21*, 639–642, doi:10.1130/0091-7613(1993)021<0639:TBAVAA>2.3.CO;2.

Malinverno, A., and L. E. Gilbert (1989), A stochastic model for the creation of abyssal hill topography at a slow spreading center, *J. Geophys. Res.*, *94*, 1665–1675, doi:10.1029/JB094iB02p01665.

Malinverno, A., and R. A. Pockalny (1990), Abyssal hill topography as an indicator of episodicity in crustal accretion and deformation, *Earth Planet. Sci. Lett.*, *99*, 154–169, doi:10.1016/0012-821X(90)90079-D.

McNutt, M. (1984), Lithospheric flexure and thermal anomalies, *J. Geophys. Res.*, *89*, 11,180–11,194, doi:10.1029/JB089iB13p11180.

Menard, H. W. (1960), The East Pacific Rise, *Science*, *132*, 1737–1746, doi:10.1126/science.132.3441.1737.

Menard, H. W. (1967), Sea floor spreading, topography, and the second layer, *Science*, *157*, 923–924, doi:10.1126/science.157.3791.923.

Mendel, V., D. Sauter, L. M. Parson, and J.-R. Vanney (1997), Segmentation and morphotectonic variations along a super-slow spreading center: The Southwest Indian Ridge (57°E–70°E), *Mar. Geophys. Res.*, *19*, 505–533, doi:10.1023/A:1004232506333.

Mendel, V., D. Sauter, C. Rommevaux-Jestin, P. Patriat, F. Lefebvre, and L. M. Parson (2003), Magmato-tectonic cyclicity at the ultra-slow spreading Southwest Indian Ridge: Evidence from variations of axial volcanic ridge morphology and abyssal hills pattern, *Geochem. Geophys. Geosyst.*, *4*(5), 9102, doi:10.1029/2002GC000417.

Meyzen, C. M., M. J. Toplis, E. Humler, J. N. Ludden, and C. Mével (2003), A discontinuity in mantle composition beneath the Southwest Indian Ridge, *Nature*, *421*, 731–733, doi:10.1038/nature01424.

Munschy, M., and R. Schlich (1990), Etude géophysique des dorsales de l'océan Indien dans la région du point triple de Rodriguez, *Oceanol. Acta*, *10*, 119–128.

Neumann, G. A., and D. W. Forsyth (1995), High resolution statistical estimation of seafloor morphology: Oblique and orthogonal fabric on the flanks of the Mid-Atlantic Ridge, 34°–35.5°S, *Mar. Geophys. Res.*, *17*, 221–250, doi:10.1007/BF01203464.

Parsons, B., and J. G. Sclater (1977), An analysis of the variation of ocean floor bathymetry and heat flow with age, *J. Geophys. Res.*, *82*, 803–827, doi:10.1029/JB082i005p00803.

Patriat, P., D. Sauter, M. Munschy, and L. M. Parson (1997), A survey of the Southwest Indian Ridge axis between Atlantis II Fracture Zone and the Indian Triple Junction: Regional setting and large scale segmentation, *Mar. Geophys. Res.*, *19*, 457–480, doi:10.1023/A:1004312623534.

Patriat, P., H. Sloan, and D. Sauter (2008), From slow to ultra-slow: A previously undetected event at the Southwest Indian Ridge at ∼24Ma, *Geology*, *36*, 207–210, doi:10.1130/G24270A.1.

Phipps Morgan, J., and Y. J. Chen (1993), The dependence of ridge-axis morphology and geochemistry on spreading rate and crustal thickness, *Nature*, *364*, 706–708, doi:10.1038/364706a0.

Poliakov, A. N. B., and W. R. Buck (1998), Mechanics of stretching elastic–plastic-viscous layers: Applications to

slow-spreading mid-ocean ridges, in *Faulting and Magmatism at Mid-Ocean Ridges*, *Geophys. Monogr. Ser.*, vol. 106, edited by W. R. Buck et al., pp. 305–323, AGU, Washington, D. C., doi:10.1029/GM106p0305.

Sauter, D., and M. Cannat (2010), The ultraslow-spreading Southwest Indian Ridge, in *Diversity of Hydrothermal Systems on Slow-Spreading Ocean Ridges*, *Geophys. Monogr. Ser.*, vol. 188, edited by P. Rona et al., pp. 153–173, AGU, Washington, D. C., doi:10.1029/2008GM000843.

Sauter, D., J.-M. Nafziger, H. Whitechurch, and M. Munschy (1996), Segmentation and morphotectonic variations of the Central Indian Ridge (21°10′S–22°25′S), *J. Geophys. Res.*, *101*, 20,233–20,256, doi:10.1029/96JB00884.

Sauter, D., P. Patriat, C. Rommevaux-Jestin, M. Cannat, and A. Briais, and the Gallieni Shipboard and Scientific Party (2001), The Southwest Indian Ridge between 49°15′E and 57°E: Focused accretion and magma redistribution, *Earth Planet. Sci. Lett.*, *192*, 303–317, doi:10.1016/S0012-821X(01)00455-1.

Sauter, D., L. M. Parson, V. Mendel, C. Rommevaux-Jestin, O. Gomez, A. Briais, C. Mével, and K. Tamaki (2002), TOBI sidescan sonar imagery of the very slow-spreading Southwest Indian Ridge: Evidence for along-axis magma distribution, *Earth Planet. Sci. Lett.*, *199*, 81–95, doi:10.1016/S0012-821X(02)00543-5.

Sauter, D., V. Mendel, C. Rommevaux-Jestin, L. M. Parson, H. Fujimoto, C. Mével, M. Cannat, and K. Tamaki (2004), Focused magmatism versus amagmatic spreading along the ultraslow-spreading Southwest Indian Ridge: Evidence from TOBI sidescan sonar imagery, *Geochem. Geophys. Geosyst.*, *5*, Q10K09, doi:10.1029/2004GC000738.

Sauter, D., M. Cannat, and V. Mendel (2008), Magnetization of 0–26.5 Ma seafloor at the ultraslow spreading Southwest Indian Ridge 61–67°E, *Geochem. Geophys. Geosyst.*, *9*, Q04023, doi:10.1029/2007GC001764.

Sauter, D., M. Cannat, C. Meyzen, A. Bezos, P. Patriat, E. Humler, and E. Debayle (2009), Propagation of a melting anomaly along the ultraslow Southwest Indian Ridge between 46°E and 52°20′E: Interaction with the Crozet hot-spot?, *Geophys. J. Int.*, *179*(2), 687–699, doi:10.1111/j.1365-246X.2009.04308.x.

Sauter, D., H. Sloan, M. Cannat, J. A. Goff, P. Patriat, M. Schaming, and W. R. Roest (2011a), From slow to ultraslow: How does spreading rate affect seafloor roughness and crustal thickness?, *Geology*, *39*, 911–914, doi:10.1130/G32028.1.

Sauter D., et al. (2011b), Mantle exhumation at the Southwest Indian Ridge: Preliminary results of the "SMOOTHSEAFLOOR" cruise, Abstract AGU2011-T15 presented at 2011 Fall Meeting, AGU, San Francisco, Calif., 5–9 Dec.

Searle, R. C., and A. Bralee (2007), Asymmetric generation of oceanic crust at the ultra-slow spreading Southwest Indian Ridge, 64°E, *Geochem. Geophys. Geosyst.*, *8*, Q05015, doi:10.1029/2006GC001529.

Searle, R. C., P. A. Cowie, N. C. Mitchell, S. Allerton, C. J. MacLeod, J. Escartín, S. M. Russell, P. A. Slootweg, and T. Tanaka (1998), Fault structure and detailed evolution of a slow spreading ridge segment: The Mid-Atlantic Ridge at 29°N, *Earth Planet. Sci. Lett.*, *154*, 167–183, doi:10.1016/S0012-821X(97)00160-X.

Searle, R. C., M. Cannat, K. Fujioka, C. Mével, H. Fujimoto, A. Bralee, and L. Parson (2003), FUJI Dome: A large detachment fault near 64°E on the very slow-spreading Southwest Indian Ridge, *Geochem. Geophys. Geosyst.*, *4*(8), 9105, doi:10.1029/2003GC000519.

Sempéré, J.-C., J. R. Cochran, and the SEIR Scientific Team (1997), The Southeast Indian Ridge between 88°E and 118°E: Variations in crustal accretion at constant spreading rate, *J. Geophys. Res.*, *102*(B7), 15,489–15,505, doi:10.1029/97JB00171.

Seyler, M., M. Cannat, and C. Mével (2003), Evidence for major-element heterogeneity in the mantle source of abyssal peridotites from the Southwest Indian Ridge (52° to 69°E), *Geochem. Geophys. Geosyst.*, *4*(2), 9101, doi:10.1029/2002GC000305.

Shaw, P. R. (1992), Ridge segmentation, faulting and crustal thickness in the Atlantic Ocean, *Nature*, *358*, 490–493, doi:10.1038/358490a0.

Shaw, P. R., and J. Lin (1993), Causes and consequences of variations in faulting style at the Mid-Atlantic Ridge, *J. Geophys. Res.*, *98*, 21,839–21,851, doi:10.1029/93JB01565.

Shaw, W. J., and J. Lin (1996), Models of ocean ridge lithospheric deformation: Dependence on crustal thickness, spreading rate, and segmentation, *J. Geophys. Res.*, *101*, 17,977–17,993, doi:10.1029/96JB00949.

Sloan, H., and P. Patriat (2004), Generation of morphotectonic fabric on the Mid-Atlantic Ridge flanks, 28° to 29°N: Implications for the limits of tectonic deformation and abyssal hill formation, *Geochem. Geophys. Geosyst.*, *5*, Q02994, doi:10.1029/2003GC000584.

Small, C. (1998), Global systematics of mid-ocean ridge morphology, in *Faulting and Magmatism at Mid-Ocean Ridges*, *Geophys. Monogr. Ser.*, vol. 106, edited by W. R. Buck et al., pp. 1–25, AGU, Washington, D. C., doi:10.1029/GM106p0001

Standish, J. J., H. J. B. Dick, P. J. Michael, W. G. Melson, and T. O'Hearn (2008), MORB generation beneath the ultraslow spreading Southwest Indian Ridge (9–25°E): Major element chemistry and the importance of process versus source, *Geochem. Geophys. Geosyst.*, *9*, Q05004, doi:10.1029/2008GC001959.

Tucholke, B. E., J. Lin, M. C. Kleinrock, M. Tivey, T. B. Reed, J. Goff, and G. E. Jaroslow (1997), Segmentation and crustal structure of the western Mid-Atlantic Ridge flank, 25°25′–27°10′N and 0–29 m.y, *J. Geophys. Res.*, *102*(B5), 10,203–10,223, doi:10.1029/96JB03896.

Weigelt, E., and W. Jokat (2001), Peculiarities of roughness and thickness of oceanic crust in the Eurasian Basin, Arctic Ocean, *Geophys. J. Int.*, *145*, 505–516, doi:10.1046/j.1365-246X.2001.00398.x.